Deletion of the Unfolded Protein Response Transducer IRE1α Is Detrimental to Aging Photoreceptors and to ER Stress-Mediated Retinal Degeneration

Dawiyat Massoudi,[1] Seán Gorman,[1] Yien-Ming Kuo,[1] Takao Iwawaki,[2] Scott A. Oakes,[3] Feroz R. Papa,[4] and Douglas B. Gould[1,5]

[1]Department of Ophthalmology, University of California, San Francisco, San Francisco, California, United States
[2]Division of Cell Medicine, Medical Research Institute, Kanazawa Medical University, Ishikawa, Japan
[3]Department of Pathology, Pritzker School of Medicine, University of Chicago, Chicago, Illinois, United States
[4]Department of Medicine, Diabetes Center, Quantitative Biosciences Institute and Lung Biology Center University of California, San Francisco, San Francisco, California, United States
[5]Department of Anatomy, Institute for Human Genetics, Cardiovascular Research Institute, Bakar Aging Research Institute, University of California, San Francisco, California, United States

Correspondence: Douglas B. Gould, Smith Cardiovascular Research Building, 555 Mission Bay Boulevard South, San Francisco, CA 94158, USA;
douglas.gould@ucsf.edu.

Received: November 8, 2022
Accepted: April 6, 2023
Published: April 25, 2023

Citation: Massoudi D, Gorman S, Kuo YM, et al. Deletion of the unfolded protein response transducer IRE1α is detrimental to aging photoreceptors and to ER stress-mediated retinal degeneration. *Invest Ophthalmol Vis Sci.* 2023;64(4):30.
https://doi.org/10.1167/iovs.64.4.30

Purpose. The unfolded protein response (UPR) is triggered when the protein folding capacity of the endoplasmic reticulum (ER) is overwhelmed and misfolded proteins accumulate in the ER, a condition referred to as ER stress. IRE1α is an ER-resident protein that plays major roles in orchestrating the UPR. Several lines of evidence implicate the UPR and its transducers in neurodegenerative diseases, including retinitis pigmentosa (RP), a group of inherited diseases that cause progressive dysfunction and loss of rod and cone photoreceptors. This study evaluated the contribution of IRE1α to photoreceptor development, homeostasis, and degeneration.

Methods. We used a conditional gene targeting strategy to selectively inactivate *Ire1α* in mouse rod photoreceptors. We used a combination of optical coherence tomography (OCT) imaging, histology, and electroretinography (ERG) to assess longitudinally the effect of IRE1α deficiency in retinal development and function. Furthermore, we evaluated the IRE1α-deficient retina responses to tunicamycin-induced ER stress and in the context of RP caused by the rhodopsin mutation Rho^{P23H}.

Results. OCT imaging, histology, and ERG analyses did not reveal abnormalities in IRE1α-deficient retinas up to 3 months old. However, by 6 months of age, the *Ire1α* mutant animals showed reduced outer nuclear layer thickness and deficits in retinal function. Furthermore, conditional inactivation of *Ire1α* in rod photoreceptors accelerated retinal degeneration caused by the Rho^{P23H} mutation.

Conclusions. These data suggest that IRE1α is dispensable for photoreceptor development but important for photoreceptor homeostasis in aging retinas and for protecting against ER stress-mediated photoreceptor degeneration.

Keywords: retinitis pigmentosa, rhodopsin, unfolded protein response, retinal degeneration, IRE1α

In eukaryotic cells, transmembrane and secreted proteins fold and mature in the lumen of the endoplasmic reticulum (ER), where they undergo a series of posttranslational modifications.[1] When the protein folding capacity of the ER is overwhelmed and misfolded proteins accumulate in the ER, the cell experiences ER stress and activates intracellular signaling pathways collectively referred to as the unfolded protein response (UPR) that aim to restore cellular homeostasis.[2,3] The UPR is initially adaptive as it attempts to reinstate ER homeostasis by increasing protein folding capacity,[4–8] reducing global protein synthesis,[9,10] and enhancing protein turnover.[2,3,11–18] However, under prolonged ER stress, when homeostasis cannot be restored, the cell triggers a pro-apoptotic signaling cascade or terminal UPR, which leads to cell death.[2,18–24]

Inositol-requiring enzyme-1 (IRE1), protein kinase RNA-like ER kinase (PERK), and activating transcription factor 6 (ATF6) are the three known UPR transducers. IRE1 is the most evolutionary conserved branch of the UPR and has two known isoforms (α and β) in mammals. Whereas IRE1β expression is restricted to the gastrointestinal tract epithelial cells[25] and bronchial epithelia,[26] IRE1α is ubiquitously expressed,[27] and its deletion in mice is embryonic lethal.[28] IRE1α possesses dual kinase and endoribonuclease activities and is activated by oligomerization and *trans*-autophosphorylation.[29] Upon mild-to-moderate activation, IRE1α initiates frame-shift splicing of *XBP1* mRNA,[30,31]

which gets translated into a transcription factor that modulates the expression of genes encoding for proteins involved in ER protein folding and quality control,[7] setting in motion a powerful adaptive response to ER stress. However, under high and chronic ER stress, IRE1α RNase relaxes its substrate specificity and cleaves many ER-localized mRNAs, including those encoding for chaperones, degrading the protein folding capacity of the ER and ultimately leading to cell death.[32,33] Although, this mechanism can be viewed as a way to protect the organism from rogue cells and their secretion of improperly folded proteins, excessive ER stress-associated cell death can cause tissue destruction and degenerative disorders such as retinitis pigmentosa (RP).[19,34–36]

RP is a group of inherited diseases that cause progressive retinal dysfunction and loss of rod and cone photoreceptors that can lead to blindness.[37] RP has a worldwide prevalence of about 1 in 4000 individuals[37,38] and has no cure. Mutations in rhodopsin are the leading cause of autosomal-dominant RP, with more than 150 distinct mutations identified to date.[39–41] Moreover, substitution of proline to histidine at amino acid 23 of rhodopsin (*Rho*^{P23H}) represents the most common RP-causing mutation in North America.[42,43] Several studies have shown that *Rho*^{P23H} mutations cause misfolding and accumulation of mutant rhodopsin in the ER that hyperactivate the UPR, including the IRE1α pathway.[43–48] Furthermore, expression of UPR pathway genes was found to be altered in *Rho*^{P23H} mutant rats.[19]

Here, we used a combination of in vivo imaging along with structural and functional assays to evaluate the role of IRE1α in photoreceptor development and homeostasis. We show that IRE1α is dispensable for rod photoreceptor development and maturation but is critical for their health and survival during aging. Importantly, our findings also reveal the protective effect of adaptive IRE1α signaling on rod photoreceptors against RP caused by *Rho*^{P23H} mutation.

Materials and Methods

Animals

Animals were housed in a 12-hour light/12-hour dark cycle environment, with food and water available ad libitum. All animals used in this study were backcrossed for at least five generations to the C57BL/6J background. *Ire1α* floxed (flox) mice were previously described.[28] *Ire1α*$^{+/flox}$ mice were crossed with *Rho-iCre*$^{+}$ mice[49] to generate *Ire1α*$^{+/flox}$; *Rho-iCre*$^{+}$ mice. These animals were then crossed to *Ire1α*$^{flox/flox}$ mice to generate the experimental mice. *Ire1α*$^{+/flox}$ mice were also bred with *Rho*$^{+/P23H}$ mice (The Jackson Laboratory, Bar Harbor, ME, USA) to generate *Ire1α*$^{+/flox}$; *Rho*$^{+/P23H}$ mutant mice that were then crossed to *Ire1α*$^{flox/flox}$; *Rho-iCre*$^{+}$ mice to obtain experimental cohorts used in this study. *Ire1α*$^{flox/flox}$; *Rho-iCre*$^{+}$ animals were also bred with the ROSA26 tdTomato reporter line[50] to generate animals used to evaluate recombination efficiency in the rod photoreceptors. C57BL/6J mice were purchased from The Jackson Laboratory. The animal protocols were approved by the Animal Care and Use Committee of the University of California, San Francisco, and are in compliance with the ARVO Statement for the Use of Animals in Ophthalmic and Vision Research.

In Vivo Imaging

The Envisu R4300 spectral-domain optical coherence tomography (SD-OCT) system (Leica/Bioptigen, Research Triangle Park, NC, USA) was used to image and measure the outer nuclear layer (ONL) and retinal thickness in vivo. Mice were anesthetized by intraperitoneal injection of ketamine and xylazine (100 mg/kg and 10 mg/kg, respectively). Pupils were dilated with 1% tropicamide, and eyes were kept hydrated with GenTeal (Alcon, Fort Worth, TX, USA). Images were acquired in rectangular volume scans to capture retinal thickness using the optic nerve as position of reference. ONL and retinal thickness were measured using the in situ calipers of the instrument before the images were saved for further analysis.

Electroretinography

Visual function was assessed by dark- and light-adapted electroretinography using the CELERIS system (Diagnosys LLC, Gaithersburg, MD, USA). Mice were dark-adapted 2.5 hours prior to the recordings. Under dim red light, mice were anesthetized by intraperitoneal injection of ketamine and xylazine (100 mg/kg and 10 mg/kg, respectively). Pupils were dilated with 1% tropicamide, and corneas were kept hydrated with 2.5% methylcellulose. A needle electrode was placed under the skin between the shoulders to serve as both reference and ground. Electroretinography (ERG) responses from both eyes were recorded simultaneously via coiled silver electrodes in contact with the cornea. Dark-adapted responses were recorded in darkness to brief white flashes (30 cd·s/m^2; seven responses were averaged for each animal with an interstimulus interval of 10 seconds). Light-adapted responses were recorded after adapting the animal to a constant white background of 30 cd/m^2; brief white flashes were delivered over the rod-saturating background (30 cd·s/m^2; seven responses were averaged for each animal with an interstimulus interval of 15 seconds). The a-wave was measured as the distance from baseline to the first negative peak present in the ERG response after delivery of the light flash, and the b-wave amplitude was measured from the a-wave to the following positive maximum peak in the ERG response.[51]

Intravitreal Injections

Mice were anesthetized with 5% isoflurane for 5 minutes and then maintained anesthetized with a constant flow of 2.5% isoflurane. After topical anesthesia with proparacaine hydrochloride, 1 µL of tunicamycin (EMD Millipore, Burlington, MA, USA) or dimethylformamide (Sigma-Aldrich, St. Louis, MO, USA) was injected into the vitreous of 1-month-old mice. SD-OCT was performed at days 7, 14, and 21 post-injection as described above.

Histology

Eyes were harvested and fixed in half-strength Karnovsky fixative (4% paraformaldehyde + 2.5% glutaraldehyde) in 0.1-M PO_4 buffer (pH 7.4) for 48 hours, dehydrated in graded ethanol, and embedded in Technovit 7100 glycol methacrylate (Electron Microscopy Sciences, Hatfield, PA, USA). Serial sagittal sections (2 µm) passing through the optic nerve head were cut and stained with hematoxylin and eosin (H&E). Images were acquired by an upright Axiophot microscope (ZEISS, Oberkochen, Germany) equipped with a 40× objective on a 12-MP Insight camera. The ONL thickness was measured at 0.25-mm increments from the optic nerve

Investigative Ophthalmology & Visual Science

toward the limbus and plotted as a spider diagram using Prism 9.4.1 software (GraphPad, La Jolla, CA, USA).

Immunohistochemistry

Eyes were harvested and embedded in Tissue-Tek Optimal Cutting Temperature (O.C.T.) compound (Sakura Finetek, Torrance, CA, USA) and directly frozen. Sections (12 µm) cut through the optic nerve head were dried at room temperature for 2 hours prior to fixation in 4% paraformaldehyde in PBS for 15 minutes, washed with PBS, blocked with 10% BSA in TBS, and incubated overnight at 4°C with anti-RFP rabbit polyclonal antibody (#600-401-379, 1:400; Rockland Immunochemicals, Pottstown, PA, USA). Sections were washed in Tris-buffered saline and Tween 20 and incubated with horseradish peroxidase (HRP)-conjugated donkey anti-rabbit secondary antibody (#711-035-152, 1:1000; Jackson ImmunoResearch Laboratories, West Grove, PA, USA) for 1 hour at room temperature. Diaminobenzidine (DAB) was used as the HRP substrate. The nuclei were counterstained with hematoxylin, and sections were mounted with Cytoseal 60 (Thermo Fisher Scientific, Waltham, MA, USA).

Polymerase Chain Reaction

Genomic DNA from 1-month-old mouse retinas was extracted with sodium hydroxide supplemented with EDTA, purified with gradients of cold ethanol, and resuspended in water. DNA (500 ng) was used to assess the excision of the *Ire1α* floxed allele in the presence of Rho-iCre as previously described.[28]

Reverse-Transcription PCR

Total RNA was isolated from 1-month-old retinas using the RNeasy Micro Kit (QIAGEN, Hilden, Germany) and reverse transcribed using the iScript cDNA Synthesis Kit (Bio-Rad, Hercules, CA, USA). SYBR GreenER qPCR SuperMix (Bio-Rad) and the following primers were used for PCR reactions: *Ire1α* forward 5′-GCTATGGATCCCCAGCAG-3′ and reverse 5′-GACTTTGTGCGCTACTTCAC-3′; and *Gapdh* forward 5′-CAATGTGTCCGTCGTGGATCTGA-3′ and reverse 5′-CTGCGACTTCAACAGCAACTC-3′.

Quantitative Real-Time PCR

Total RNA was isolated from 1-month-old retinas using the RNeasy Micro Kit and reverse transcribed using the iScript cDNA Synthesis Kit. Quantitative PCR (qPCR) was performed on a Bio-Rad CFX384 real-time system using SsoFast EvaGreen Supermix (Bio-Rad) and the following primers: *Hspa5* forward 5′-CCTGCGTCGGTGTGTTCAAG-3′ and reverse 5′-AAGGGTCATTCCAAGTGCG-3′; total-*Xbp1* forward 5′- GAAAAACAGAGTAGCAGCGCAGA-3′ and reverse 5′-CCCAAGCGTGTTCTTAACTC-3′; *Atf4* forward 5′-AAACCTCATGGGTTCTCCAG-3′ and reverse 5′-GGCATGGTTTCCAGGTCATC-3′; *Ddit3* forward 5′-ACGGAAACAGAGTGGTCAGTGC-3′ and reverse 5′-CAGGAGGTGATGCCCACTGTTC-3′; and *Rpl19* forward 5′- ATGCCAACTCCCGTCAGCAG-3’ and reverse 5′-TCATCCTTCTCATCCAGGTCACC-3′. Then, 10 ng of cDNA and 1 µM of primers were used per reaction in a final volume of 10 µL. Each sample was run in duplicate. The relative expression of each gene was normalized to *Rpl19* and analyzed using the $2^{-\Delta\Delta CT}$ method.

Immunoblotting

Proteins from 1-month-old retinas were extracted in 50 µL ice-cold RIPA Buffer (Sigma-Aldrich) supplemented with proteinases inhibitors and EDTA and were centrifuged at 13000 rpm for 10 minutes at 4°C. The supernatant was collected, and protein samples were separated on an Invitrogen NuPAGE 4 to 12%, Bis-Tris gel (Thermo Fisher Scientific) and transferred to polyvinylidene fluoride (PVDF) membranes. Membranes were blocked in 5% non-fat milk (Bio-Rad) and incubated overnight with anti-IRE1α (#3294, 14C10, rabbit mAb, 1:1000; Cell Signaling Technology, Danvers, MA, USA) or anti α-tubulin (#3873, DM1A, mouse mAb, 1:5000; Cell Signaling Technology) antibodies. Membranes were washed in TBS–Tween 20 and incubated with HRP-conjugated secondary antibodies (donkey anti-rabbit or anti-mouse IgG, 711-035-152 and 715-035-150, 1:10,000; Jackson ImmunoResearch Laboratories) for 1 hour at room temperature. Proteins were detected using the Immobilon Forte Western HRP Substrate (Sigma-Aldrich).

Statistical Analysis

Statistical analyses were performed using Prism 9.4.1. Statistical comparisons between two groups were performed using two-tailed Student's *t*-tests. Multiple-group comparisons were performed using two-way ANOVA followed by post hoc Tukey's multiple comparisons tests. The data are presented as mean ± SEM for each group. $P < 0.05$ was considered significant ($^{*}P < 0.05$, $^{**}P < 0.01$, $^{***}P < 0.001$, $^{****}P < 0.0001$).

Results

Rho-iCre Mediates Inactivation of *Ire1α* in Mouse Rod Photoreceptors

To determine the role of IRE1α in photoreceptor development and homeostasis, we crossed an *Ire1α* conditional null allele[28] to the Rho-iCre (Cre) line[49] to selectively inactivate *Ire1α* in rod photoreceptors. Recombination was assessed by PCR, RT-PCR, and western blot analysis. PCR analysis of both genomic DNA and cDNA clearly showed robust recombination and generation of an excised allele in the presence of Cre (Figs. 1A–1C). The intensity of the excised band was greater in the homozygous *Ire1α* floxed mice compared to heterozygous mice and absent in the Cre-negative samples, further supporting the specificity of the observed results. Furthermore, IRE1α immunoblotting revealed a significant reduction of IRE1α protein in retinas from heterozygous knockout mice that was further reduced in the homozygous mutant animals (Fig. 1D). *Ire1α* deletion is expected to occur only in rod photoreceptors, which represent approximately 70% of total murine retinal cells.[52,53] Therefore, we still expect *Ire1α* transcript and protein products from the remaining cell types, hence the noticeable amounts of transcripts and proteins in the homozygous samples (Figs. 1C, 1D). We validated these observations by crossing the $Ire1\alpha^{flox/flox}$; $Rho\text{-}iCre^{+}$ mice with a ROSA26 tdTomato reporter mouse line.[50] Retinal immunohistochemical labeling for tdTomato showed a positive signal in the presence of Cre only, providing further evidence of the Cre activity and therefore excision of the *Ire1α* allele in rod photoreceptors (Fig. 1E, right panel). Collectively, these results show

Investigative Ophthalmology & Visual Science

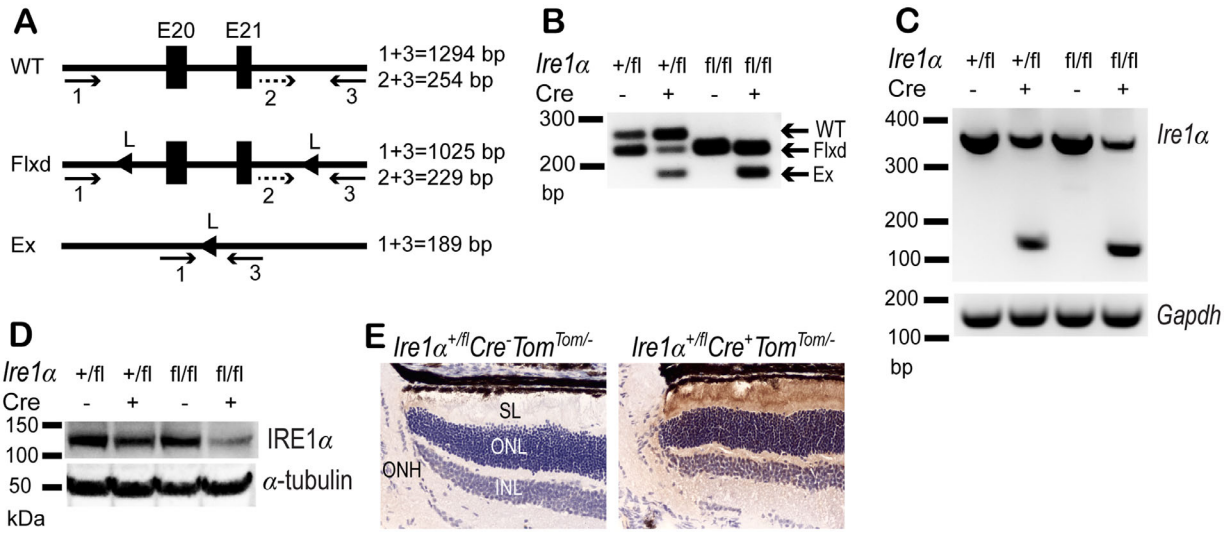

Figure 1. Conditional inactivation of *Ire1α* in mouse rod photoreceptors by Rho-iCre. (**A**) Conditional *Ire1α* mutant allele showing the locations of LoxP sites (*arrowheads*) and primers (*arrows*) used for PCR (shown in **B**). (**B**, **C**) Excision of *Ire1α* at the DNA and mRNA levels, respectively, in 1-month-old retinas. Note the intensity of the excised band that is brighter in the homozygous than in the heterozygous retinas and absent in the control samples as expected. (**D**) Representative IRE1α immunoblotting shows a similar pattern whereby the IRE1α levels are much lower in the homozygous than in the heterozygous retinas. The presence of unexcised products in the homozygous samples in **B** and **C** and the detectable amount of protein in the homozygous samples in **D** can be attributed to other retinal cell types that do not express the Rho-iCre recombinase (Cre). (**E**) Representative images of immunohistochemical staining of retinas from *Ire1α* mutant mice carrying the ROSA26 tdTomato reporter showing labeling of the tdTomato fluorescent protein (DAB staining) only in the presence of the Cre (*right*). E, exon; L, LoxP site; Flxd, floxed; Ex, excised; ONH, optic nerve head; SL, segment layer; ONL, outer nuclear layer; INL, inner nuclear layer.

successful excision of *Ire1α* by Rho-iCre in the mouse rod photoreceptors.

IRE1α-Deficient Retinas Experience Age-Related Degeneration

To assess the consequences of IRE1α deficiency on retinal development, we carried out a longitudinal study where we analyzed retinas using OCT imaging and histology in mice at 1, 3, 6, 9, and 12+ months old (Fig. 2). OCT at early time points (1 and 3 months) did not detect abnormalities in the IRE1α-deficient retinas (Figs. 2A–2C). However, in retinas 6 months and older, we observed a steady decrease in retinal thickness that was attributable to ONL thinning (Figs. 2A–2E). The retinal degeneration observed was progressive and affected males and females at similar rates (Fig. 2; Supplementary Figs. S1A–S1D). Consistent with the OCT findings, histological analysis of retinas 3 and 12+ months old did not reveal abnormalities at 3 months but showed ONL thinning and excess rod photoreceptors loss at 12+ months in both heterozygous and homozygous mutant retinas (Figs. 2F–2H). In summary, these data show that the absence of IRE1α in murine rod photoreceptors does not impact retinal development but becomes detrimental to photoreceptors survival after 3 months of age.

To gain insight into how the loss of IRE1α in rod photoreceptors does not cause abnormalities in young retinas, we performed qPCR analysis to evaluate the expression of genes downstream of ATF6 (*Hspa5* and *Xbp1*) and PERK (*Atf4* and *Ddit3*) in 1-month-old IRE1α-deficient retinas. The results did not reveal changes in the expression of *Hspa5* and *Xbp1*. However, the expression of *Atf4* showed a significant increase and *Ddit3* expression remained unchanged (Supplementary Fig. S2). These data suggest that the absence of IRE1α may be compensated by an increase in the PERK pathway in young retinas. Furthermore, expression of the pro-apoptotic gene *Ddit3* encoding C/EBP homologous protein (CHOP) was unchanged, consistent with the absence of photoreceptor loss in IRE1α mutant retinas at 1 month of age (Supplementary Fig. S2).

IRE1α Deficiency in Rod Photoreceptors Induces Functional Retinal Deficits

To determine whether inactivation of *Ire1α* in rod photoreceptors induces visual impairment, we assessed retinal function by ERG whereby we performed scotopic ERG to evaluate rod and cone function and photopic ERG to selectively assess the function of cone photoreceptors. Compared to control littermates, scotopic and photopic ERG responses of 3-month-old IRE1α-deficient retinas did not reveal dysfunction (Fig. 3), suggesting that the photoreceptors function normally in these animals. However, by 6 months of age, the scotopic ERG recordings showed a reduction in photoreceptor responses in retinas from heterozygous and homozygous mutant mice (Figs. 3A–3E), but their photopic ERG responses did not show any significant difference (Figs. 3F–3J). This suggests that functional retinal deficits at this age are mainly driven by the loss and/or dysfunction of the rod photoreceptors. Furthermore, scotopic and photopic retinal responses were comparable between males and females of a given genotype (Figs. 3D, 3E, 3I, 3J; Supplementary Figs. S3A–S3D). Together, these results show that IRE1α deficiency in rod photoreceptors leads to age-related visual impairments that occur between 3 and 6 months old.

Investigative Ophthalmology & Visual Science

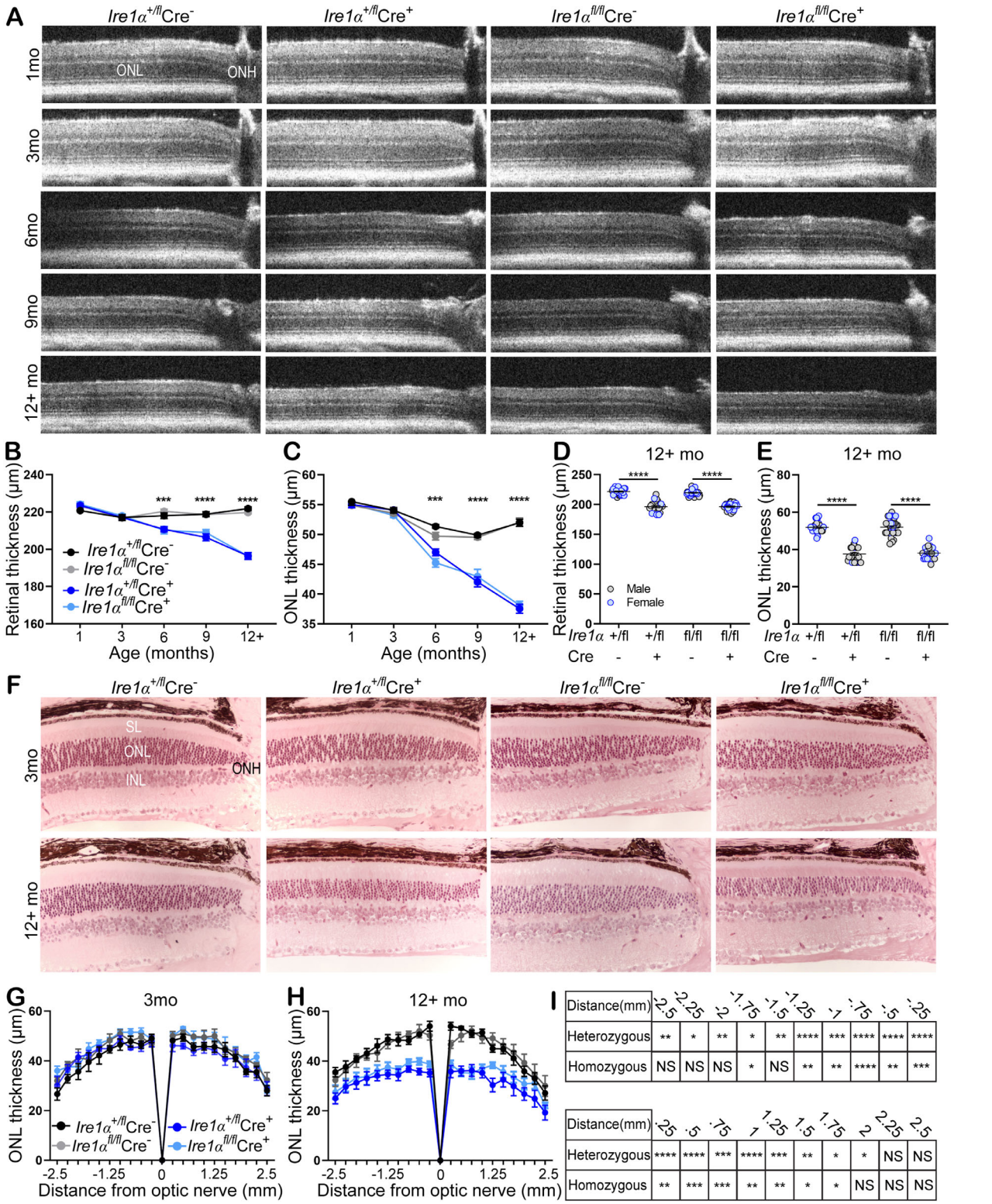

Figure 2. IRE1α deficiency in rod photoreceptors induces age-related retinal degeneration. (**A**) OCT images of IRE1α-deficient retinas 1, 3, 6, 9, and 12+ months old showing progressive retinal and ONL thinning of both *Ire1α* heterozygous and homozygous mutant mice starting between 3 and 6 months old. (**B**) Retinal thickness. (**C**) ONL thickness. (**D**, **E**) Distribution of retinal and ONL thickness of *Ire1α* mutant mice at 12+ months old. There is no difference between male and female mice (n = 17–26 at 1 month; n = 16–42 at 3 months; n = 16–35 at 6 months; n = 16–24 at 9 months, and n = 23–36 at +12 months; see also Supplementary Fig. S1). (**F**) H&E staining shows a reduction of retinal and ONL thickness in eyes from IRE1α-deficient animals at 12+ months old but there was no sign of degeneration at 3 months. (**G**, **H**) Quantification of ONL thickness in retinas 3 and 12+ months old measured from H&E-stained sections, respectively (n = 4–6 at 3 months and n = 6–9 at 12+ months). (**I**) Statistical results of data represented in **H**. Data in **B** to **E** are presented as mean ± SEM. *P < 0.05, **P < 0.01, ***P < 0.001, ****P < 0.0001; two-tailed Student's t-test. ONH, optic nerve head; SL, segment layer; ONL, outer nuclear layer; INL, inner nuclear layer; NS, not significant.

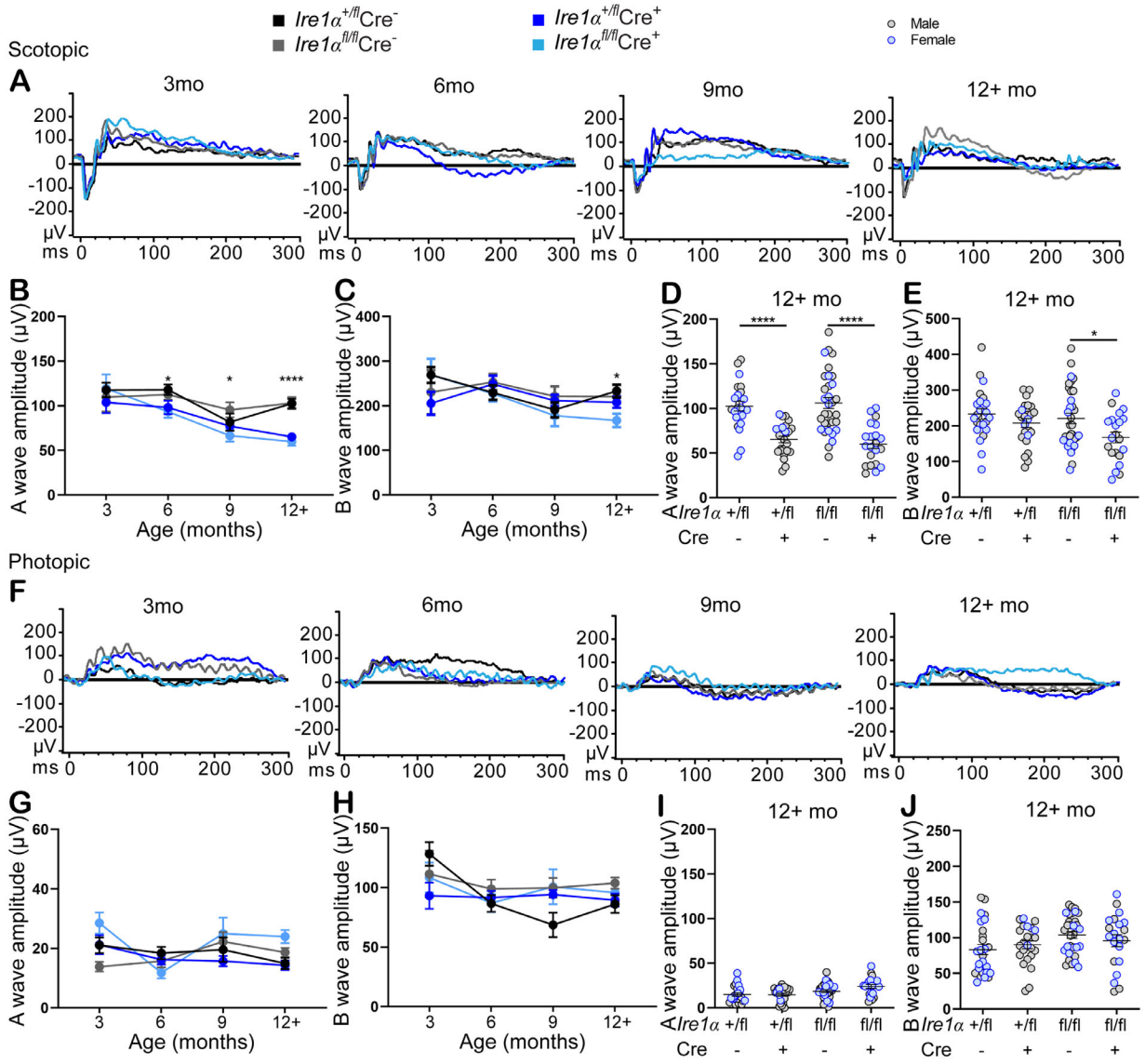

Figure 3. ERG recordings show functional retinal deficits after conditional inactivation of *Ire1α* in rod photoreceptors. (**A**) Scotopic ERG recordings at different ages and their a-wave (**B**) and b-wave (**C**) amplitudes over time show unchanged retinal function among genotypes at 3 months old but show progressive decreased responses in *Ire1α* mutant retinas at 6, 9, and 12+ months of age (**A–E**). (**D**, **E**) Scotopic responses of males and females at 12+ months showing equivalent distributions within both sexes. (**F**) Photopic ERG recordings of IRE1α-deficient retinas at various ages and their a-wave (**G**) and b-wave (**H**) amplitudes did not reveal any differences at any given time points (**F–J**). (**I**, **J**) Photopic responses of males and females at 12+ months show no difference between sexes (n = 8–16 at 3 months; n = 14–21 at 6 months; n = 8–24 at 9 months, and n = 21–32 at 12+ months; see also Supplementary Fig. S3). Data in **B** to **E** and **G** to **J** are presented as mean ± SEM. *$P \leq 0.05$, ****$P < 0.0001$; two-tailed Student's t-test.

IRE1α Deficiency in Rod Photoreceptors Does Not Affect Retinal Degeneration Caused by Chemically Induced ER Stress

Tunicamycin induces protein misfolding and ER stress by inhibiting N-linked protein glycosylation within the ER.[54–56] Depending on its activation level, IRE1α can mediate adaptive or apoptotic responses,[57] and our previous work showed that preventing high-level IRE1α activation by pharmacologically blocking its kinase-dependent oligomerization protects against tunicamycin-induced cell death.[58] Thus, we tested whether *Ire1α* inactivation is protective or detrimental to photoreceptors after ER stress induced by tunicamycin. We first evaluated the effects of intravitreal injection of different concentrations of tunicamycin (5, 10, and 20 µg/mL) on wild-type mouse retinas to determine an optimal concentration to efficiently induce ER stress without inducing a severe and rapid cell death. Tunicamycin induced dose-dependent retinal degeneration within 14 days of injection (Figs. 4A, 4B). Because all three tunicamycin concentrations tested caused retinal degeneration, we used 5 µg/mL of tunicamycin to assess the consequences of pharmacologically inducing ER stress in IRE1α-deficient retinas. The analysis performed by OCT at days 7, 14 and 21 post-tunicamycin injection did not reveal differences among the different groups of mice (Figs. 4C–4E). We next treated a second cohort of mice with the intermediate tunicamycin concentration (10 µg/mL) and found a small reduction of retinal

Investigative Ophthalmology & Visual Science

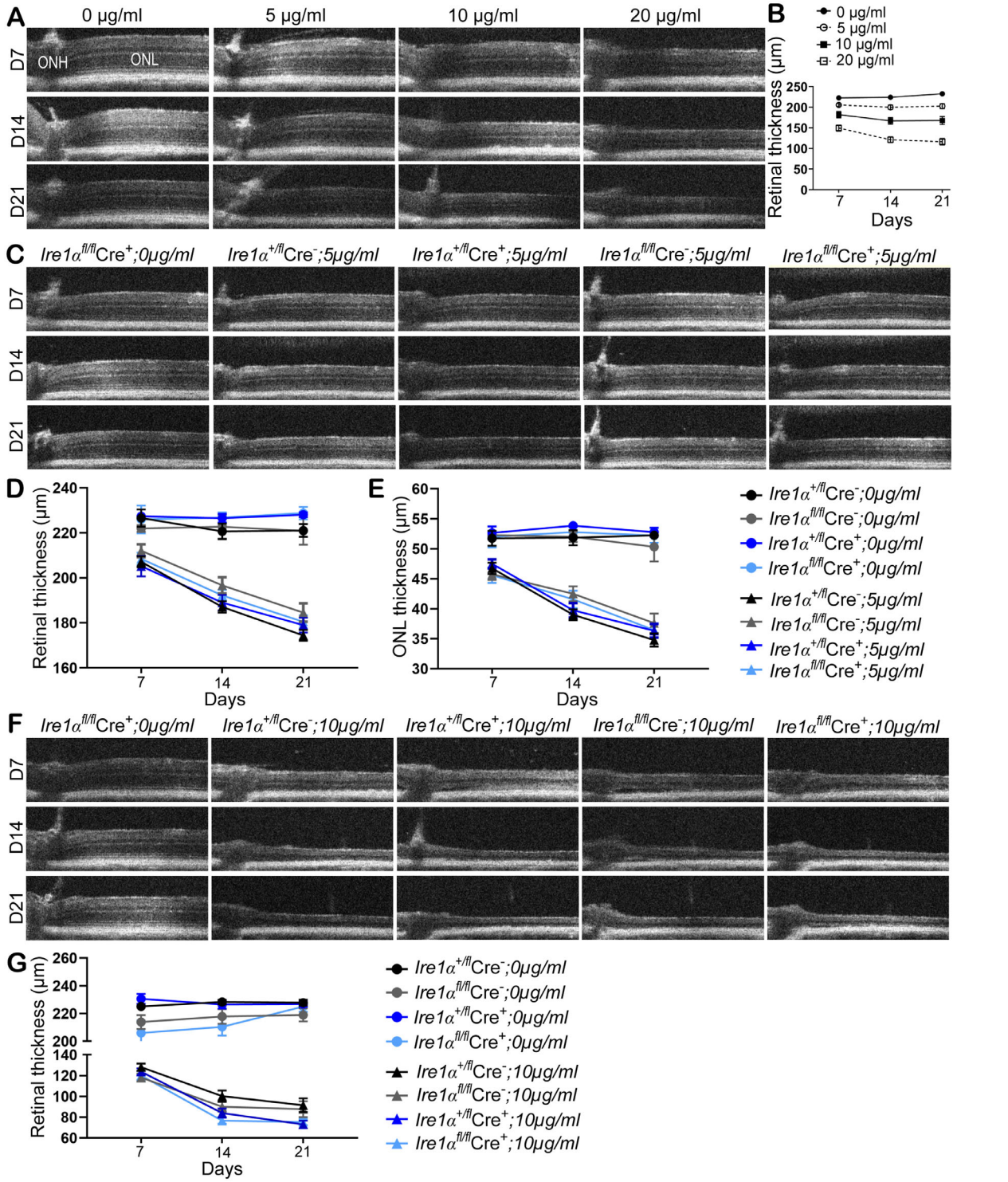

Figure 4. IRE1α deficiency in rod photoreceptors does not affect retinal degeneration caused by chemically induced ER stress. (**A**) OCT images of 1-month-old wild-type mice at days 7, 14, and 21 after intravitreal injection of different concentrations of tunicamycin (5, 10, and 20 µg/mL). (**B**) Measurements of retinal thickness at days 7, 14, and 21. (**C**) OCT images of 1-month-old *Ire1α* mutant retinas at days 7, 14, and 21 after intravitreal injection of 5 µg/mL of tunicamycin. (**D**, **E**) Retinal thickness and ONL thickness, respectively, do not show differences among the groups. (**F**) OCT images of 1-month-old *Ire1α* mutant retinas at days 7, 14, and 21 after intravitreal injection of 10 µg/mL of tunicamycin. (**G**) The small reduction of retinal thickness of IRE1α-deficient mice at day 21 post-tunicamycin injection is not statistically significant when compared to the controls. For **A** and **B**, $n = 6$–11; for **C** to **E**, $n = 5$–12; and for **F** and **G**, $n = 3$–12 (see also Supplementary Fig. S4). Data in **D**, **E**, and **G** are presented as mean ± SEM (two-way ANOVA).

thickness at day 21 in IRE1α-deficient eyes compared to their respective controls; however, it was not statistically significant (Figs. 4F, 4G; Supplementary Fig. S4C). Similar changes of retinal thickness between males and females

Investigative Ophthalmology & Visual Science

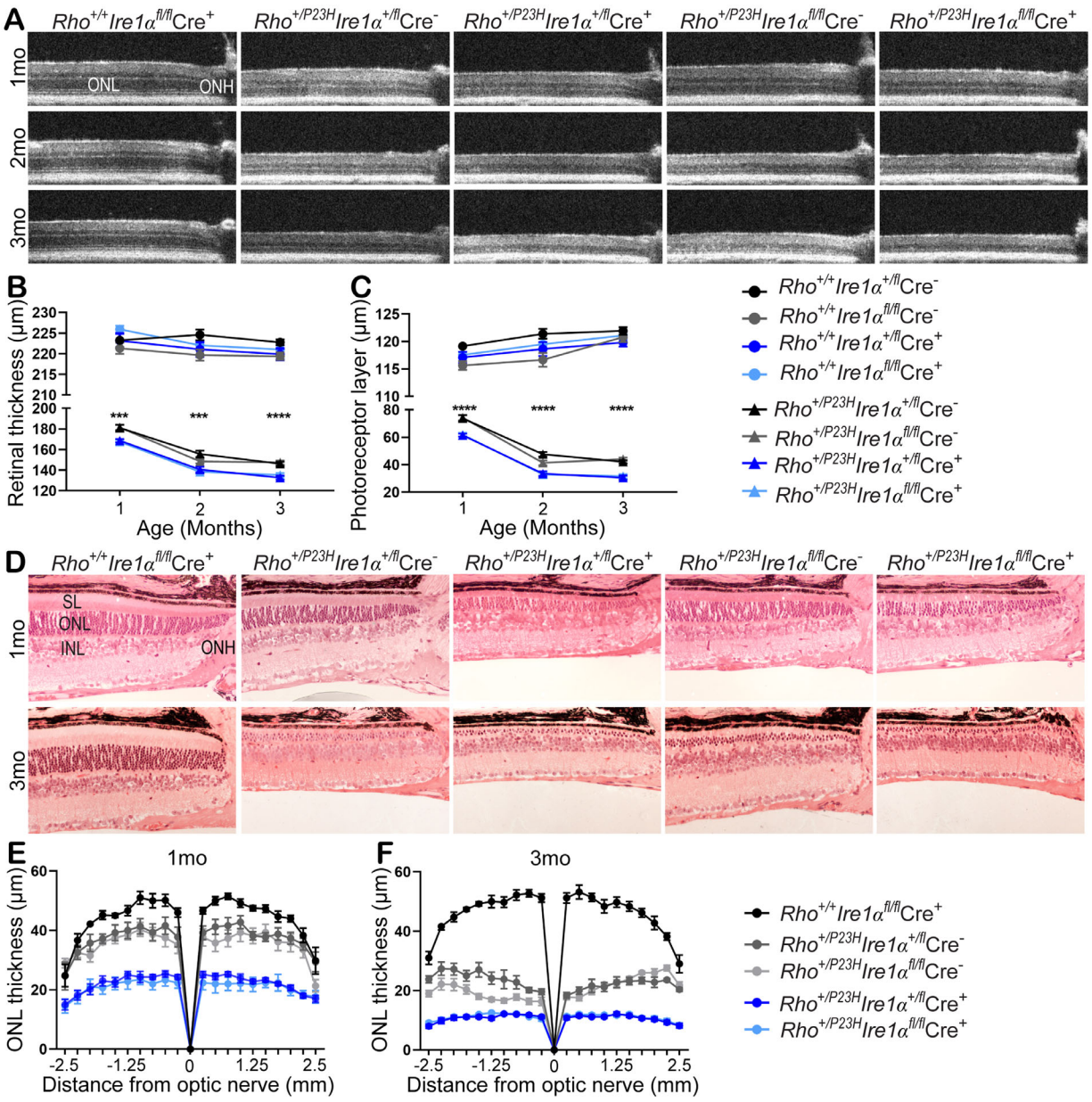

Figure 5. IRE1α deficiency in rod photoreceptors exacerbates retinal degeneration caused by the Rho^{P23H} mutation. (**A**) OCT images of IRE1α-deficient retinas at 1, 2, and 3 months old in $Rho^{+/P23H}$ or $Rho^{+/+}$ background that show retinal degeneration caused by Rho^{P23H} mutation exacerbated by the absence of IRE1α in rod photoreceptors. (**B**, **C**) Retinal thickness and photoreceptor layer thickness, respectively. (**D**) H&E-stained sections from 1- and 3-month-old retinas showing greater photoreceptor loss in the retinas carrying both Rho^{P23H} mutation and *Ire1α* deficiency compared to the Rho^{P23H} mutation alone or to $Rho^{+/+}$ mice. (**E**, **F**) ONL thickness of 1- and 3-month-old retinas of various genotypes, respectively. For **A** to **C**, n = 9–23 at 1 month; n = 7–16 at 2 months, and n = 10–22 at 3 months (see also SupplementaryFig. S5). For **D** to **F**, n = 5–6 at 1 and 3 months old). Data in **B** and **C** are presented as mean ± SEM. ***$P < 0.001$, ****$P < 0.0001$ (two-way ANOVA).

were observed (Supplementary Figs. S4A–S4C). In summary, these data suggest that IRE1α deficiency in rod photoreceptors does not significantly affect the retinal response to acute tunicamycin-induced degeneration.

IRE1α Deficiency in Rod Photoreceptors Accelerates Photoreceptor Loss Caused by the Rho^{P23H} Mutation

Several studies have shown that mutations in rhodopsin, including Rho^{P23H}, induce ER stress and trigger the UPR.[46,47,59] To further examine the role of IRE1α in retinal degeneration, we evaluated the consequences of *Ire1α* deficiency in a genetic model of retinal degeneration using Rho^{P23H} mutant mice. The OCT data at 1, 2, and 3 months old showed accelerated retinal degeneration in Rho^{P23H} mutant mice that were also deficient for *Ire1α* (Figs. 5A–5C). Histological analysis further confirmed the retinal thinning and showed an excessive loss of photoreceptors in the double mutant animals as early as 1 month old (Figs. 5D–5F). Similar distribution among the males and the females was observed throughout the different time points (Supplementary Figs. S5A–S5C). These results further demonstrate the

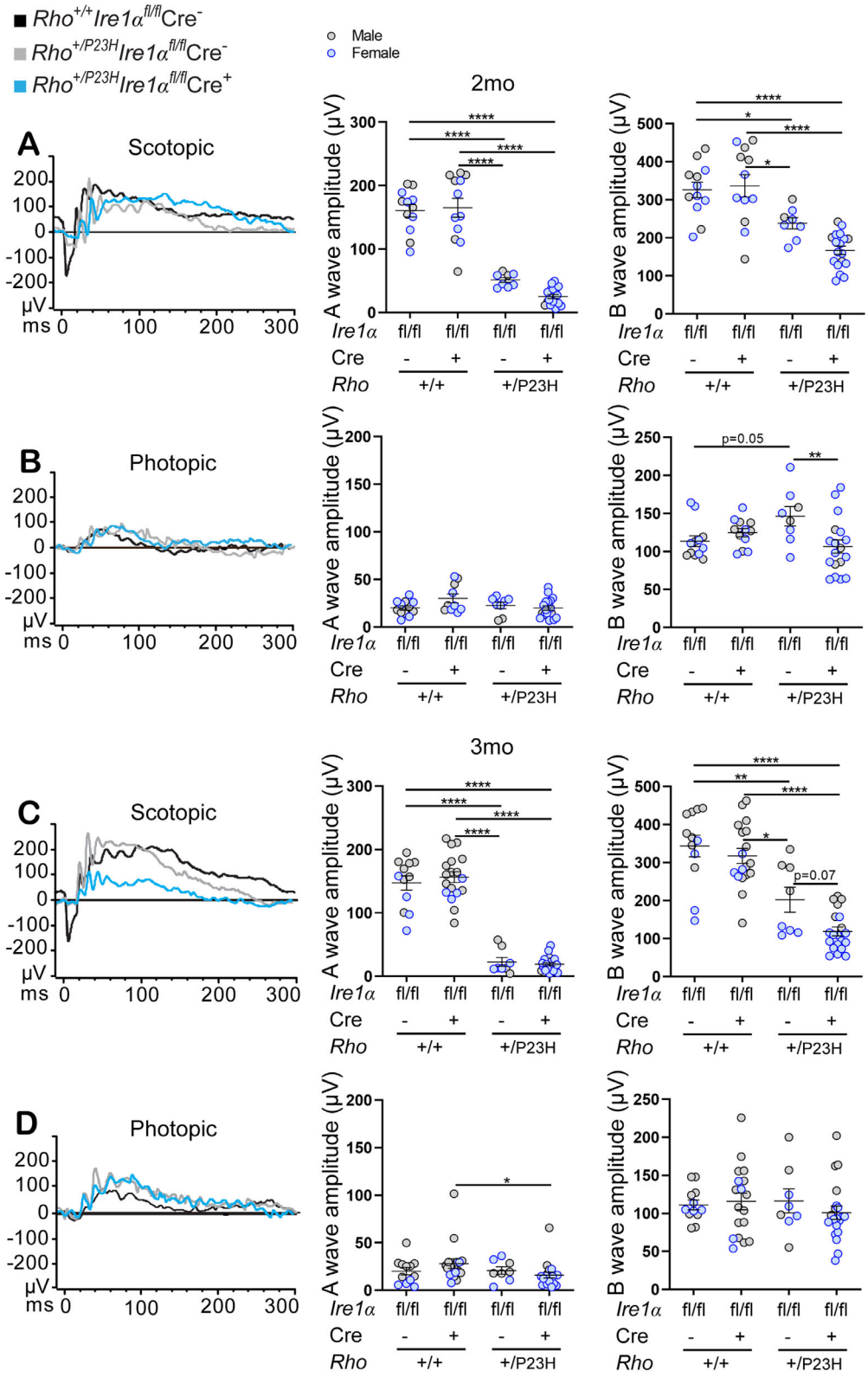

Figure 6. ERG recordings show increased retinal functional deficits in double mutant Rho^{P23H} and IRE1α-deficient retinas compared to mice carrying only the Rho^{P23H} mutation. (**A**) Scotopic ERG recordings at 2 months showing that Rho^{P23H} animals had decreased a-waves as expected and that a-wave responses tended to be further decreased in the animals with *Ire1α* deficiency. (**C**) By 3 months of age, the homozygous *Ire1α* deficiency had no impact on control mice or on the diminished scotopic a-wave amplitudes of Rho^{P23H} mice. The bipolar cell activity driven by the photoreceptors was also altered at 2 and 3 months in Rho^{P23H} mice with *Ire1α* deficiency (**A**, **C**, scotopic b-wave amplitude), demonstrating further alterations in the visual system. (**B**, **D**) Photopic ERG recordings at 2 and 3 months old, respectively, showing that *Ire1α* deficiency decreased b-wave amplitudes in eyes from Rho^{P23H} mice only at 2 months old. For **A** and **B**, $n = 8–18$; for **C** and **D**, $n = 8–20$. Data in **A** to **D** are presented as mean ± SEM. $^{*}P < 0.05$, $^{**}P < 0.01$, $^{****}P < 0.0001$ (two-way ANOVA).

Investigative Ophthalmology & Visual Science

importance of IRE1α in modulating the photoreceptors ER stress response and its protective role against ER stress-related retinal degeneration.

IRE1α Deficiency in Rod Photoreceptors Exacerbates Functional Retinal Deficits Caused by the *Rho*^{P23H} Mutation

To determine whether the effect of IRE1α deficiency on ER stress-related retinal degeneration observed by OCT and histology was also associated with visual impairments, we performed scotopic and photopic ERGs on 2- and 3-month-old retinas (Fig. 6, Supplementary Fig. S6). We detected a significantly decreased scotopic a-wave response in all *Rho*^{P23H} mice that appeared to be slightly exacerbated in 2-month-old mice that were also *Ire1α* deficient (Fig. 6A; Supplementary Fig. S6A, a-wave amplitude). By 3 months of age, heterozygous or homozygous *Ire1α* deficiency had no impact on a-wave amplitudes in control or *Rho*^{P23H} mice (Fig. 6C; Supplementary Fig. S6C, a-wave amplitude). These changes in photoreceptor responses were also accompanied by a reduction in photoreceptor-mediated bipolar cell responses (Figs. 6A, 6C; Supplementary Figs. S6A, S6C, b-wave amplitude), highlighting additional alterations in the vision circuit. The photopic responses at 2 and 3 months old remained overall unaltered in these mice (Figs. 6B, 6D; Supplementary Figs. S6B, S6D) with the exception of a decrease in the b-wave amplitude of some genotypes (Figs. 6B, 6D, b-wave amplitude). These observations suggest that the observed retinal dysfunction is mainly caused by rod photoreceptor impairment. Taken together, these data show that the absence of IRE1α in rod photoreceptors exacerbates visual impairments caused by the *Rho*^{P23H} mutation.

Discussion

Misfolded proteins and hyperactivation of the UPR are associated with many neurodegenerative diseases, including RP. For example, several RP disease-causing mutations in rhodopsin (*Rho*^{T17M}, *Rho*^{P23H}, *Rho*^{Y178C}, *Rho*^{C185R}, and *Rho*^{D190G}) lead to misfolding and retention of rhodopsin in the ER and subsequent hyperactivation of the UPR that might play major roles in photoreceptor loss.[42,46,59–61] However, how misfolded rhodopsin and hyperactivation of UPR contribute to the clinical manifestations of RP remains poorly understood. We have shown previously that a small molecule kinase inhibitor of IRE1α that prevents RNase hyperactivation and apoptotic signaling significantly reduces photoreceptor loss in *Rho*^{P23H} mutant rats.[58] In the present study, we investigated the effects of IRE1α deficiency on retinal development and homeostasis and showed that loss of IRE1α in rod photoreceptors leads to progressive photoreceptor degeneration starting between 3 and 6 months of age that is correlated with significant visual functional deficits. In addition, we show that IRE1α deficiency exacerbates retinal degeneration caused by *Rho*^{P23H} mutation.

Our findings indicate that IRE1α deficiency in rod photoreceptors does not affect retinal development or homeostasis in young animals. The absence of retinal defects in these mice up to 3 months old was unexpected given the daily burden of rhodopsin production on rod photoreceptors and the important role of IRE1α on mediating ER stress responses. However, because IRE1α is not the only UPR transducer in mammals, compensatory effects by PERK and/or ATF6 are possible in rod photoreceptors during development. Consistent with this possibility, we found a significant increase in expression of the PERK target *Atf4* in 1-month-old *Ire1a* mutant retinas. Similar behavior is observed in regulation of insulin biosynthesis in pancreatic beta cells where PERK is essential and solicited at very low glucose concentrations, whereas IRE1α in contrast is required in the presence of much higher glucose concentrations.[62–64] Therefore, our results suggest that loss of IRE1α may be compensated by PERK in young photoreceptors.

Although IRE1α-deficient retinas develop normally, they undergo progressive photoreceptor loss associated with a decrease in visual functions by 6 months of age, suggesting a crucial role of IRE1α in protecting photoreceptors against ER stress-associated age-related degeneration. Similar observations have been made with XBP1 knockout in the whole retina where structural and functional defects were only observed at around 12 to 14 months.[65] Furthermore, using an in vivo fluorescent IRE1α activity reporter (ERAI reporter mice), we previously showed a significant increase in fluorescence as the mice got older in the absence of chemical or genetic ER stress inducers,[47] reinforcing the likelihood that increasing ER stress in aging retinas triggers the activation of IRE1α. Moreover, a recent study showed that the IRE1α/XBP1 axis is required for mammalian brain aging homeostasis, as IRE1α deletion accelerated age-related cognitive decline and XBP1 overexpression reduced cell senescence and restored synaptic and cognitive function.[66] In addition, in Caenorhabditis *elegans*, a decline in the fidelity of protein quality control and protein homeostasis regulatory mechanisms with age causes increased ER stress levels concomitant with an accumulation of misfolded proteins.[67,68] Therefore, our results suggest that IRE1α is not required or its absence can be compensated for during homeostatic/normal ER stress in photoreceptors, but it is increasingly important during aging when cells experience higher levels of ER stress.

Another interesting finding from our study supports a crucial role of IRE1α signaling in protecting photoreceptors against genetically induced ER stress in young animals. Indeed, we found that IRE1α deficiency in rod photoreceptors by itself did not lead to retinal abnormalities before 3 months of age but exacerbated retinal degeneration in 1-month-old mice carrying the *Rho*^{P23H} mutation. These findings complement our previous work showing that blocking IRE1α hyperactivation by inhibiting its kinase domain protects against ER stress-induced retinal degeneration.[58] The ability of a small molecule kinase inhibitor to titrate down IRE1α activation from its apoptotic to adaptive signaling modes is distinct from genetically reducing *Ire1α* as we have done here. However, together these findings suggest that IRE1α protects rod photoreceptors against elevated ER stress up to a certain level, and hence genetic inactivation of *Ire1α* and its adaptive outputs exacerbates photoreceptor loss from ER stress associated with aging or the *Rho*^{P23H} mutation. However, as we previously showed, if ER stress is so severe and chronic that it causes IRE1α to oligomerize and its RNase to become hyperactivated, then the apoptotic outputs of IRE1α contribute to photoreceptor death and retinal degeneration.[58]

Another interesting observation is the lack of detectable phenotypic differences between heterozygous and homozygous IRE1α-deficient retinas. Indeed, the age-related retinal degeneration and the excess photoreceptor loss observed in the presence of the *Rho*^{P23H} mutation similarly affected

Investigative Ophthalmology & Visual Science

the heterozygous and homozygous retinas where one would have expected a more severe phenotype in the homozygous. This haploinsufficiency effect suggests that photoreceptors rely upon having both copies of *Ire1α* to adaptively preserve photoreceptor health and is distinct from the observation that genetic removal of *Ire1α* in other tissues such as pancreatic beta cells or lung epithelium is tolerable for cell viability.[69,70] This may be related to the extremely high expression of IRE1α in rod photoceptors compared to most cells in the body, such that even a partial loss in its expression is incompatible with the ability of the secretory pathway to keep up with demand.[47] Further investigations are necessary to unravel the molecular mechanisms behind these observations.

Acknowledgments

The authors thank Luca Della Santina, PhD, for guidance with ERG recordings, and we thank Cassandre Labelle-Dumais, PhD, and Mao Mao, PhD, for their help and comments on the manuscripts.

Supported by grants from the National Institutes of Health (R01EY027810 to S.A.O., F.R.P., D.B.G.; R01CA219815 to S.A.O.; U01DK127786 to S.A.O.; U01DK123609 to F.R.P.; R01 DK100623 to F.R.P.; R01DK129935 to F.R.P.); by a UCSF Vision Core grant (NIH/NEI P30 EY002162); and by an unrestricted grant from Research to Prevent Blindness.

Disclosure: **D. Massoudi**, None; **S. Gorman**, None; **Y.-M. Kuo**, None; **T. Iwawaki**, None; **S.A. Oakes**, OptiKira (F); **F.R. Papa**, OptiKira (F); **D.B. Gould**, None

References

1. Hebert DN, Molinari M. In and out of the ER: Protein folding, quality control, degradation, and related human diseases. *Physiol Rev*. 2007;87:1377–1408.
2. Walter P, Ron D. The unfolded protein response: From stress pathway to homeostatic regulation. *Science*. 2011;334:1081–1086.
3. Ron D, Walter P. Signal integration in the endoplasmic reticulum unfolded protein response. *Nat Rev Mol Cell Biol*. 2007;8:519–529.
4. Sriburi R, Jackowski S, Mori K, Brewer JW. XBP1: A link between the unfolded protein response, lipid biosynthesis, and biogenesis of the endoplasmic reticulum. *J Cell Biol*. 2004;167:35–41.
5. Bommiasamy H, Back SH, Fagone P, et al. ATF6α induces XBP1-independent expansion of the endoplasmic reticulum. *J Cell Sci*. 2009;122:1626–1636.
6. Schuck S, Prinz WA, Thorn KS, Voss C, Walter P. Membrane expansion alleviates endoplasmic reticulum stress independently of the unfolded protein response. *J Cell Biol*. 2009;187:525–536.
7. Lee AH, Iwakoshi NN, Anderson KC, Glimcher LH. Proteasome inhibitors disrupt the unfolded protein response in myeloma cells. *Proc Natl Acad Sci USA*. 2003;100:9946–9951.
8. Acosta-Alvear D, Zhou Y, Blais A, et al. XBP1 controls diverse cell type- and condition-specific transcriptional regulatory networks. *Mol Cell*. 2007;27:53–66.
9. Harding HP, Zhang Y, Ron D. Protein translation and folding are coupled by an endoplasmic-reticulum-resident kinase. *Nature*. 1999;397:271–274.
10. Harding HP, Novoa I, Zhang Y, et al. Regulated translation initiation controls stress-induced gene expression in mammalian cells. *Mol Cell*. 2000;6:1099–1108.
11. Travers KJ, Patil CK, Wodicka L, Lockhart DJ, Weissman JS, Walter P. Functional and genomic analyses reveal an essential coordination between the unfolded protein response and ER-associated degradation. *Cell*. 2000;101:249–258.
12. Bernales S, McDonald KL, Walter P. Autophagy counterbalances endoplasmic reticulum expansion during the unfolded protein response. *PLoS Biol*. 2006;4:e423.
13. Smith MH, Ploegh HL, Weissman JS. Road to ruin: Targeting proteins for degradation in the endoplasmic reticulum. *Science*. 2011;334:1086–1090.
14. Schuck S, Gallagher CM, Walter P. ER-phagy mediates selective degradation of endoplasmic reticulum independently of the core autophagy machinery. *J Cell Sci*. 2014;127:4078–4088.
15. Khaminets A, Heinrich T, Mari M, et al. Regulation of endoplasmic reticulum turnover by selective autophagy. *Nature*. 2015;522:354–358.
16. Fumagalli F, Noack J, Bergmann TJ, et al. Translocon component Sec62 acts in endoplasmic reticulum turnover during stress recovery. *Nat Cell Biol*. 2016;18:1173–1184.
17. Grumati P, Morozzi G, Holper S, et al. Full length RTN3 regulates turnover of tubular endoplasmic reticulum via selective autophagy. *eLife*. 2017;6:e25555.
18. Karagoz GE, Aragon T, Acosta-Alvear D. Recent advances in signal integration mechanisms in the unfolded protein response. *F1000Res*. 2019;8:F1000.
19. Lin JH, Li H, Yasumura D, et al. IRE1 signaling affects cell fate during the unfolded protein response. *Science*. 2007;318:944–949.
20. Lu M, Lawrence DA, Marsters S, et al. Opposing unfolded-protein-response signals converge on death receptor 5 to control apoptosis. *Science*. 2014;345:98–101.
21. Tabas I, Ron D. Integrating the mechanisms of apoptosis induced by endoplasmic reticulum stress. *Nat Cell Biol*. 2011;13:184–190.
22. Hetz C. The unfolded protein response: Controlling cell fate decisions under ER stress and beyond. *Nat Rev Mol Cell Biol*. 2012;13:89–102.
23. Maurel M, Chevet E, Tavernier J, Gerlo S. Getting RIDD of RNA: IRE1 in cell fate regulation. *Trends Biochem Sci*. 2014;39:245–254.
24. Hetz C, Papa FR. The unfolded protein response and cell fate control. *Mol Cell*. 2018;69:169–181.
25. Bertolotti A, Wang X, Novoa I, et al. Increased sensitivity to dextran sodium sulfate colitis in IRE1β-deficient mice. *J Clin Invest*. 2001;107:585–593.
26. Martino MB, Jones L, Brighton B, et al. The ER stress transducer IRE1β is required for airway epithelial mucin production. *Mucosal Immunol*. 2013;6:639–654.
27. Miyoshi K, Katayama T, Imaizumi K, et al. Characterization of mouse Ire1α: Cloning, mRNA localization in the brain and functional analysis in a neural cell line. *Brain Res Mol Brain Res*. 2000;85:68–76.
28. Iwawaki T, Akai R, Yamanaka S, Kohno K. Function of IRE1α in the placenta is essential for placental development and embryonic viability. *Proc Natl Acad Sci USA*. 2009;106:16657–16662.
29. Shamu CE, Walter P. Oligomerization and phosphorylation of the Ire1p kinase during intracellular signaling from the endoplasmic reticulum to the nucleus. *EMBO J*. 1996;15:3028–3039.
30. Yoshida H, Matsui T, Yamamoto A, Okada T, Mori K. XBP1 mRNA is induced by ATF6 and spliced by IRE1 in response to ER stress to produce a highly active transcription factor. *Cell*. 2001;107:881–891.
31. Calfon M, Zeng H, Urano F, et al. IRE1 couples endoplasmic reticulum load to secretory capacity by processing the XBP-1 mRNA. *Nature*. 2002;415:92–96.

32. Han D, Lerner AG, Vande Walle L, et al. IRE1α kinase activation modes control alternate endoribonuclease outputs to determine divergent cell fates. *Cell*. 2009;138:562–575.
33. Hollien J, Lin JH, Li H, Stevens N, Walter P, Weissman JS. Regulated Ire1-dependent decay of messenger RNAs in mammalian cells. *J Cell Biol*. 2009;186:323–331.
34. Chiang WC, Kroeger H, Sakami S, et al. Robust endoplasmic reticulum-associated degradation of rhodopsin precedes retinal degeneration. *Mol Neurobiol*. 2015;52:679–695.
35. Hetz C, Saxena S. ER stress and the unfolded protein response in neurodegeneration. *Nat Rev Neurol*. 2017;13:477–491.
36. Lee EJ, Chan P, Chea L, Kim K, Kaufman RJ, Lin JH. ATF6 is required for efficient rhodopsin clearance and retinal homeostasis in the P23H rho retinitis pigmentosa mouse model. *Sci Rep*. 2021;11:16356.
37. Hartong DT, Berson EL, Dryja TP. Retinitis pigmentosa. *Lancet*. 2006;368:1795–1809.
38. Pagon RA. Retinitis pigmentosa. *Surv Ophthalmol*. 1988;33:137–177.
39. Athanasiou D, Aguila M, Bellingham J, et al. The molecular and cellular basis of rhodopsin retinitis pigmentosa reveals potential strategies for therapy. *Prog Retin Eye Res*. 2018;62:1–23.
40. Kennan A, Aherne A, Humphries P. Light in retinitis pigmentosa. *Trends Genet*. 2005;21:103–110.
41. Berger W, Kloeckener-Gruissem B, Neidhardt J. The molecular basis of human retinal and vitreoretinal diseases. *Prog Retin Eye Res*. 2010;29:335–375.
42. Sung CH, Davenport CM, Hennessey JC, et al. Rhodopsin mutations in autosomal dominant retinitis pigmentosa. *Proc Natl Acad Sci USA*. 1991;88:6481–6485.
43. Tam BM, Moritz OL. Characterization of rhodopsin P23H-induced retinal degeneration in a *Xenopus laevis* model of retinitis pigmentosa. *Invest Ophthalmol Vis Sci*. 2006;47:3234–3241.
44. Liu X, Garriga P, Khorana HG. Structure and function in rhodopsin: Correct folding and misfolding in two point mutants in the intradiscal domain of rhodopsin identified in retinitis pigmentosa. *Proc Natl Acad Sci USA*. 1996;93:4554–4559.
45. Frederick JM, Krasnoperova NV, Hoffmann K, et al. Mutant rhodopsin transgene expression on a null background. *Invest Ophthalmol Vis Sci*. 2001;42:826–833.
46. Gorbatyuk MS, Knox T, LaVail MM, et al. Restoration of visual function in P23H rhodopsin transgenic rats by gene delivery of BiP/Grp78. *Proc Natl Acad Sci USA*. 2010;107:5961–5966.
47. Alavi MV, Chiang WC, Kroeger H, et al. In vivo visualization of endoplasmic reticulum stress in the retina using the ERAI reporter mouse. *Invest Ophthalmol Vis Sci*. 2015;56:6961–6970.
48. Athanasiou D, Aguila M, Bellingham J, Kanuga N, Adamson P, Cheetham ME. The role of the ER stress-response protein PERK in rhodopsin retinitis pigmentosa. *Hum Mol Genet*. 2017;26:4896–4905.
49. Li S, Chen D, Sauve Y, McCandless J, Chen YJ, Chen CK. Rhodopsin-iCre transgenic mouse line for Cre-mediated rod-specific gene targeting. *Genesis*. 2005;41:73–80.
50. Madisen L, Zwingman TA, Sunkin SM, et al. A robust and high-throughput Cre reporting and characterization system for the whole mouse brain. *Nat Neurosci*. 2010;13:133–140.
51. McCulloch DL, Marmor MF, Brigell MG, et al. ISCEV Standard for full-field clinical electroretinography (2015 update). *Doc Ophthalmol*. 2015;130:1–12.
52. Jeon CJ, Strettoi E, Masland RH. The major cell populations of the mouse retina. *J Neurosci*. 1998;18:8936–8946.
53. Hughes AE, Enright JM, Myers CA, Shen SQ, Corbo JC. Cell type-specific epigenomic analysis reveals a uniquely closed chromatin architecture in mouse rod photoreceptors. *Sci Rep*. 2017;7:43184.
54. Surani MA. Glycoprotein synthesis and inhibition of glycosylation by tunicamycin in preimplantation mouse embryos: Compaction and trophoblast adhesion. *Cell*. 1979;18:217–227.
55. Yoo J, Mashalidis EH, Kuk ACY, et al. GlcNAc-1-P-transferase–tunicamycin complex structure reveals basis for inhibition of N-glycosylation. *Nat Struct Mol Biol*. 2018;25:217–224.
56. Hakulinen JK, Hering J, Branden G, et al. MraY–antibiotic complex reveals details of tunicamycin mode of action. *Nat Chem Biol*. 2017;13:265–267.
57. Chen Y, Brandizzi F. IRE1: ER stress sensor and cell fate executor. *Trends Cell Biol*. 2013;23:547–555.
58. Ghosh R, Wang L, Wang ES, et al. Allosteric inhibition of the IRE1α RNase preserves cell viability and function during endoplasmic reticulum stress. *Cell*. 2014;158:534–548.
59. Jiang H, Xiong S, Xia X. Retinitis pigmentosa-associated rhodopsin mutant T17M induces endoplasmic reticulum (ER) stress and sensitizes cells to ER stress-induced cell death. *Mol Med Rep*. 2014;9:1737–1742.
60. Illing ME, Rajan RS, Bence NF, Kopito RR. A rhodopsin mutant linked to autosomal dominant retinitis pigmentosa is prone to aggregate and interacts with the ubiquitin proteasome system. *J Biol Chem*. 2002;277:34150–34160.
61. Liu H, Wang M, Xia CH, et al. Severe retinal degeneration caused by a novel rhodopsin mutation. *Invest Ophthalmol Vis Sci*. 2010;51:1059–1065.
62. Moore CE, Omikorede O, Gomez E, Willars GB, Herbert TP. PERK activation at low glucose concentration is mediated by SERCA pump inhibition and confers preemptive cytoprotection to pancreatic beta-cells. *Mol Endocrinol*. 2011;25:315–326.
63. Lipson KL, Fonseca SG, Ishigaki S, et al. Regulation of insulin biosynthesis in pancreatic beta cells by an endoplasmic reticulum-resident protein kinase IRE1. *Cell Metab*. 2006;4:245–254.
64. Hassler JR, Scheuner DL, Wang S, et al. The IRE1α/XBP1s pathway is essential for the glucose response and protection of β cells. *PLoS Biol*. 2015;13:e1002277.
65. McLaughlin T, Falkowski M, Park JW, et al. Loss of XBP1 accelerates age-related decline in retinal function and neurodegeneration. *Mol Neurodegener*. 2018;13:16.
66. Cabral-Miranda F, Tamburini G, Martinez G, et al. Unfolded protein response IRE1/XBP1 signaling is required for healthy mammalian brain aging. *EMBO J*. 2022;41:e111952.
67. Henis-Korenblit S, Zhang P, Hansen M, et al. Insulin/IGF-1 signaling mutants reprogram ER stress response regulators to promote longevity. *Proc Natl Acad Sci USA*. 2010;107:9730–9735.
68. Taylor RC, Dillin A. XBP-1 is a cell-nonautonomous regulator of stress resistance and longevity. *Cell*. 2013;153:1435–1447.
69. Lee H, Lee YS, Harenda Q, et al. Beta cell dedifferentiation induced by IRE1α deletion prevents type 1 diabetes. *Cell Metab*. 2020;31:822–836.e5.
70. Auyeung VC, Downey MS, Thamsen M, et al. IRE1α drives lung epithelial progenitor dysfunction to establish a niche for pulmonary fibrosis. *Am J Physiol Lung Cell Mol Physiol*. 2022;322:L564–L580.

Investigative Ophthalmology & Visual Science